Fully-Optoelectronic 300 GHz Multi-Channel Wireless Link Using a Photonically-Pumped Low-Barrier Mixer for up to 180 Gbps

Iñigo Belio-Apaolaza, Javier Martinez-Gil, Jonas Tebart, Jose Luis Fernández Estévez, Marcel Grzeslo, Diego Moro-Melgar, Oleg Cojocari, Andreas Stöhr, *Senior Member, IEEE*, and Cyril C. Renaud, *Senior Member, IEEE,*

***Abstract*—Wireless communications at 300 GHz are expected to play an important role in the deployment of 6G and beyond networks. Multiple electronic and photonic technologies compete in this regard, each bringing its own particular benefits. While purely optoelectronic links are interesting for incorporating photonic advantages in signal transmission and reception, electronic receivers typically based on Schottky mixers are far superior in conversion efficiency. Thus, the link signal-to-noise ratio (SNR) is improved, and higher throughput can be achieved. Here, we demonstrate a fully-optoelectronic 300 GHz band multi-channel link using a novel low-barrier Schottky mixer driven with a photonically generated local oscillator (LO) signal in the receiver using a modified uni-travelling-carrier photodiode (MUTC-PD). This combines the efficient down-conversion of Schottky-based mixers and the advantages of photonic LO signals such as tuneability, remote generation and distribution, and the reuse of coherent technology used in fibre networks. Up to three frequency channels are generated in the transmitter which is also based on a MUTC-PD photomixer. We achieve a maximum aggregate line rate of 180 Gbps over a distance of 1.5 meters, utilizing 16-QAM format and optical intensity modulation. The transmission operates within the soft-decision forward error correction (SD-FEC) limit, with each channel being received sequentially.**

***Index Terms*—Terahertz photonics, microwave photonics, terahertz communications, photonic local oscillator, optoelectronic mixing, low-barrier Schottky mixer, radio-over-fibre.**

I. Introduction

In response to the ever-increasing demand for high-speed data transmission, terahertz band (0.1-10 THz) communications have been widely investigated and constitute a very active area of research at the present time [1]–[3]. Currently, future ultra-dense 6G networks are the primary driving force. As the number of deployed cells and connections grows exponentially, such dense networks will not rely exclusively on optical fibre for backhaul or fronthaul links [4]–[6], where the deployment of fibre may be cost-inefficient and inconvenient. In this sense, wireless connections at THz bands could satisfy the needs of the network, providing fast links ($>$ 100 Gbps) and complementing the optical network where required [7], [8]. Nevertheless, the convergence between fibre and wireless links will be of major importance, leading to high-speed, low-latency, and low-power communications [7], [9]. Data centres have also brought the attention of the THz community to solving a similar problem [10], [11]. In an ultra-dense data centre, fibre connections become problematic as the cables can obstruct air flows of refrigeration, challenge reconfigurability, and limit the space available in the rack [12]–[14]. Inter-rack wireless links are envisioned as a potential solution where needed, and in this sense the THz band is capable of providing enough bandwidth. Among the terahertz range, the 220-330 GHz band shows great potential to be used in future networks for these purposes. This is due to the large available bandwidth, the low atmospheric attenuation, and the advances in key technologies. These discussed prospects have materialized in the first standardization steps with the IEEE 802.15.3d standard between 252 and 325 GHz [15].

A wide variety of technologies have been studied for THz communications. These can be categorized into three groups: purely electronic [16]–[19], hybrid electronic-photonic [20]–[23], and purely optoelectronic [24]–[26]. The use of optoelectronic technologies is especially interesting for several compelling reasons. Among them, we can highlight the high tuneability of sources, the reuse of mature and cost-effective coherent technology of optical networks, and the low-loss distribution of signals via optical fibres [27]. Therefore a purely optoelectronic solution is potentially the best suited for the needs discussed previously. However, the hybrid electronic-photonic approach currently dominates the field in terms of high data rates, achieving up to 1 Tbps recently employing MIMO and polarization multiplexing [28]. The key terahertz technologies in hybrid electronic-photonic systems are uni-traveling-carrier-photodiodes (UTC-PDs) as photonic to terahertz converters in the transmitter, and GaAs-based Schottky mixers as terahertz down-converters in the receiver.

Purely optoelectronic links substitute the electronic mixer with an optoelectronic mixer, typically based on an ultra-fast photoconductor, which is a scheme commonly found in ultra-broadband spectroscopy systems [29]–[31]. This option offers immense receiver tuneability, and the LO signals can be distributed over fibre, simplifying the terahertz front-ends

Manuscript received XXXX XX, 2023; revised XXXX XX, 2023. This work was supported by Horizon 2020 Marie Skodowska-Curie Actions project TERAOPTICS (956857) and by the German Federal Ministry of Education and Research (BMBF) within the project 6GEM (16KISK039). (*Corresponding author: Iñigo Belio-Apaolaza)*

I. Belio-Apaolaza and C. C. Renaud are with the Department of Electronic and Electrical Engineering, University College London, London WC1E 7JE, U.K. (e-mail: inigo.apaolaza.21@ucl.ac.uk; c.renaud@ucl.ac.uk).

J. Martinez-Gil, D. Moro-Melgar and O. Cojocari are with ACST GmbH, Josef-Bautz-Str. 15, 63457 Hanau, Germany (e-mail: javier.martinez-gil@acst.de; diego.moro-melgar@acst.de; oleg.cojocari@acst.de).

J. Tebart, J.L. Fernández Estévez, M. Grzeslo, and A. Stöhr are with the Institute of Optoelectronics, University of Duisburg-Essen, 47057 Duisburg, Germany (e-mail: jonas.tebart@uni-due.de; jose.fernandez-estevez@uni-due.de; marcel.grzeslo@uni-due.de; andreas.stoehr@uni-due.de).

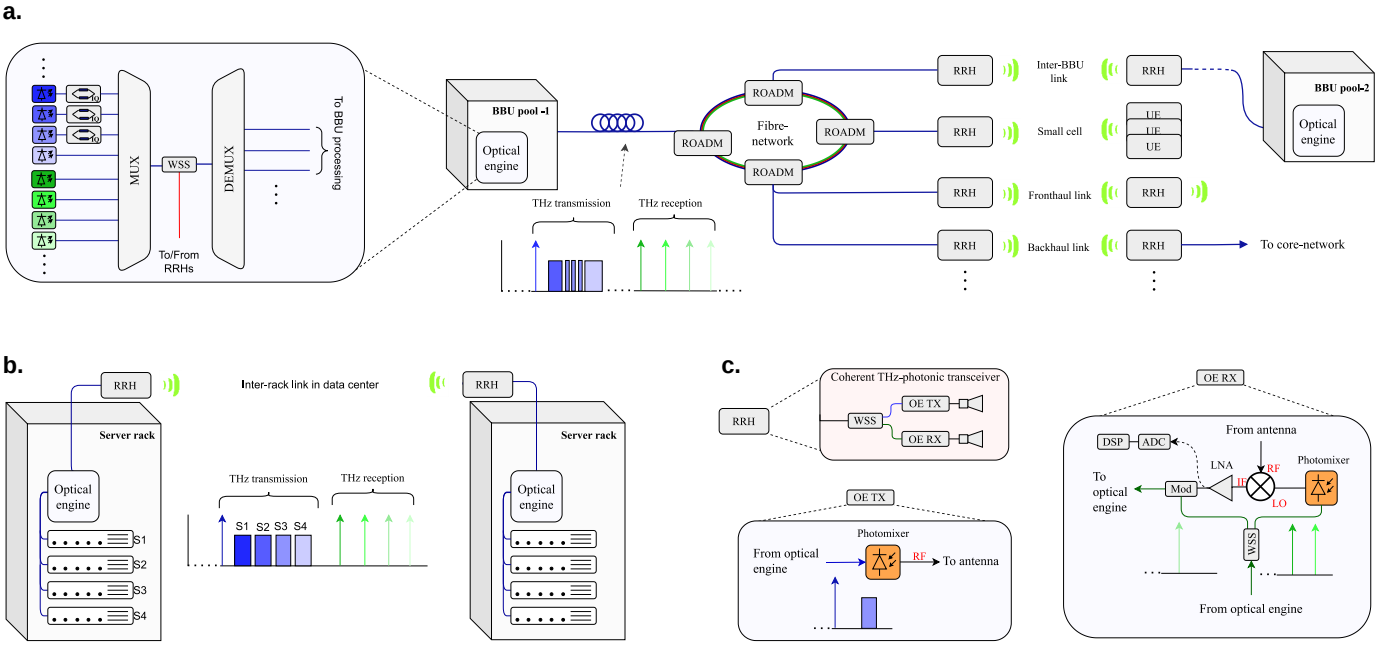

Fig. 1. Simplified concept and applications of coherent THz photonic transceivers in future C-RAN based networks and data centres: **a.** The BBUs include optical engines responsible of generating the different THz channels and the THz LOs to operate in full-duplex mode. This is distributed via the local fibre network to the RRHs, e.g. inter-BBU links, small cell links or backhaul links. Each RRH can operate in single-channel or multi-channel modes, covering multiple THz bands with the same optical engine at the BBU. **b.** The same concept can be applied to data centres for inter-rack links. In this example, the rack has four server units (S1 to S4) which are connected to the optical engine via their optical interface. The data of each server unit is transmitted at a different frequency channel and received through the photonic LOs which can be easily reconfigured. **c.** The RRH's key component is a coherent THz photonic transceiver in which the receiver part down-converts the THz signal and sends it back to the BBU, both parts utilizing the remote photonic LO received from the BBUs. WSS: Wavelength selective switch, ROADM: Reconfigurable optical add and drop multiplexer, RRH: Remote radio head, BBU: Baseband unit, UE: User equipment, ADC: Analog to digital converter, DSP: Digital signal processing, LNA: Low-noise amplifier, OE: Optoelectronic.

TABLE I
COMPARISON OF FULLY-OPTOELECTRONIC TERAHERTZ LINKS WITH A HETERODYNE RECEIVER. ZBD: ZERO BIAS DETECTOR.

Reference	Centre frequency (GHz)	Modulation format	Total rate (Gbps)	Wireless distance (m)	Optical distance (km)	THz amplification	Real-time	Receiver type
[25]	80 to 320	BPSK	0.1	0.1	-	No	Yes	Photoconductor
[26]	90 to 310	QPSK	3.2	1	-	No	Yes	Photoconductor
[36]	120	QPSK	10	1	-	No	No	Photoconductor
[37]	120/320	QPSK	12/4	1	-	No	No	Photoconductor
[24]	306	QPSK	30(1)	58	-	Yes	No	Photoconductor
[38]	300	QPSK	40	52	-	Yes	No	ZBD + photonic LO
[39]	262	8/16-QAM	45	1	5	No	No	GaAs Schottky mixer + photonic LO
[40]	355	16-QAM	60	4	25	No	No	GaAs Schottky mixer + photonic LO
This work	280	16-QAM	100(2)/180(1)	1.5	-	No	No	InGaAs Schottky mixer + photonic LO

(1) Multi-channel transmission with sequentially received channels. (2) Single-channel transmission.

by eliminating the need for an electronic LO source typically based on power-hungry active multiplier chains. However, the conversion efficiency is significantly lower than with Schottky mixers [32]–[34]. Therefore, purely optoelectronic links based in a down-conversion scheme have not yet demonstrated data rates comparable to using electronic mixers. In table I a summary of this type of fully-optoelectronic demonstrations is shown. Alternatively, direct THz-to-optical conversion has recently shown high potential reaching throughputs of 240/190 Gbps for 5/110 m of wireless distance utilizing a plasmonic modulator and THz amplifiers [35].

Regarding heterodyne receiver based systems, a solution that has been minimally investigated consists of driving an electronic mixer with a photonically generated LO. This can combine the efficient down-conversion of electronic mixers with the photonic advantages previously highlighted. To illustrate the potential use of this type of receiver, we show in figure 1.**a.** a simplified vision of a future cloud radio access network (C-RAN), utilizing fully-optoelectronic terahertz solutions and facilitating fibre-wireless convergence. In the baseband unit (BBU) pools, optical engines are responsible for generating the different terahertz channels with complex IQ modulation and the terahertz LOs. These signals are distributed via a local fibre network covering a particular set of front-ends, which

are constituted by remote radio heads (RRH). Here, the key component is the colorless optoelectronic terahertz transceiver, in which the receiver is based on an electronic mixer driven with photonically generated LO in a photomixer. The down-converted signal is sent back to the BBU modulating an optical carrier directly, or it can be digitally processed first if a digitized radio-over-fibre (DRoF) solution is used. Although each RRH would cover a particular terahertz band, limited by the mixer and/or amplifiers, the optical engine can cover multiple bands up to several THz thanks to the ultra-wide tuneability of lasers. Here optical sources are free-running lasers for simplicity, but phase-locked sources such as optical frequency combs (OFC) could also be used. The same concept can be applied to inter-rack communications in data centres with transparent wireless bridges, as illustrated in figure 1.**b.**

Recently this type of terahertz optoelectronic receiver was demonstrated using a novel 300 GHz subharmonic InGaAs Schottky mixer driven with a photonic LO generated in a UTC-PD [41], [42]. Thanks to its low-barrier height the mixer can be driven directly with a single UTC-PD, heterodyning two lasers separated by the LO frequency. In comparison, the LO requirements of a GaAs mixer detriments the functionality of an optically-pumped receiver by driving the mixer with non-optimal power [39], or requiring additional LO amplification [40]. Here, we use a photonically-driven InGaAs mixer and go a step further, demonstrating multi-channel 300 GHz transmission using a 16-QAM modulation format, achieving a maximum data rate of 180 Gbps over 1.5 m, using free-running lasers and optical intensity modulation. This is to the best of the authors' knowledge a record for fully-optoelectronic terahertz links with heterodyne receivers, and also a record using intensity-modulated optical signals in the context of terahertz communications.

II. Methods

A. Transmitter setup

The experimental setup of the 300 GHz link is depicted in figure 2.**a**. The data to be transmitted is generated with a Fujitsu FPGA board with 88 Gsamples/s digital-to-analog converters (DACs), designed for use in optical networks. The data consists of a random sequence of 10000 symbols encoded in 16-QAM gray format which is sampled at the FPGA rate, and raised-cosine (RC) filtered with a roll-off factor (α) of 0.1. The complex baseband IQ waveform is then digitally upconverted to a frequency $f_{up} = R_s/2 + 1.5\,\text{GHz}$ where R_s is the baseband data bandwidth in GHz which is equal to the baud rate. A pre-emphasis filter is used to boost the high frequencies and compensate for the roll-off of RF cables. After the digital-to-analog conversion, the signal is amplified by 28 dB (SHF 810) and drives a Mach-Zehnder modulator (MZM) (FUJITSU FTM 7938 EZ) with 40 GHz RF bandwidth.

To generate the different frequency channels, up to three free-running tuneable external-cavity lasers (ECL) (IDPhotonics CoBrite DX2-S and PurePhotonics PPCL200) with 80 kHz linewidth are modulated by the MZM. In this way, all modulated lasers transport the same data, which is done to reduce the complexity of the setup. The use of optical heterodyning and coherent reception allows the bias of the MZM to be set near the null point, exploiting a greater signal excursion. After modulation, the optical signals go through an erbium-doped fibre amplifier (EDFA) (Thorlabs EDFA100P) and are combined with an additional laser, i.e. the photonic local oscillator (CoBrite DX2-S, LD-1 in the schematic), separated by the desired THz frequency. In figure 2.**c.** examples of the resulting optical spectrum are depicted for the cases of using single, dual, and triple channel configurations.

The power of the combined optical signals is adjusted with a variable optical attenuator (VOA) and then amplified again by a second EDFA (IPG Laser GmbH EAD-500-CL) resulting in 20 dBm of optical power. The VOA also allows to monitor and limit the input power of the second EDFA. This amplifier feeds the optical-to-terahertz converter, which is based on a $5\text{x}30\,\mu\text{m}^2$ MUTC-PD chip probed with a GSG WR-3.4 probe (Cascade InfinityProbe) (see figure 2.**b.** top-right). The MUTC-PD design and fabrication details can be found in [43]. To couple the light to the integrated optical waveguide, we use a lensed fibre, as shown in figure 2.**b.** (bottom). A WR-3.4 horn antenna is used at the output of the probe followed by a 5 cm diameter PTFE lens (Thorlabs PTFE LAT100). The bias voltage of the MUTC-PD is fixed at -2 V. The power of the specific MUTC-PD used was not measured, but measurements on same batch devices reveal a power of approximately -18 dBm at 280 GHz and 10 mA of photocurrent [44]. This value is calculated from the measured power at 30 mA (-3 dBm) and corrected with the measured probe losses. The photocurrent is limited to 10 mA to avoid saturating the low-barrier mixer, as will be discussed later.

B. Receiver setup

On the receiver side, the key component is a novel subharmonic low-barrier Schottky mixer [41]. In contrast to conventional THz Schottky mixers which are based on GaAs contacts, here we use InGaAs, resulting in a barrier height of 0.2-0.3 eV compared to 0.8-0.9 eV of GaAs metal-semiconductor rectifying contacts. This translates to a significant relaxation in LO power requirements, to approximately 200 uW, which is one and two orders of magnitude lower than in narrow-band and full-band GaAs mixers respectively [45]–[48]. The mixer is packaged in a rectangular waveguide block with WR3.4 access for the RF, WR6 for the LO, and a high-frequency SMA connector for the IF. The mixer features a conversion loss and noise figure of about 16 dB, and an IF bandwidth of 23 GHz. More details about the performance and characterization with a photonic LO can be found in [41], [42], [49].

The low-power LO requirement enables the use of photomixing in the generation of the LO signal, providing enough power to saturate conversion loss and reducing the power consumption [49]. This is done using a second probed MUTC-PD chip with lensed fibre and driven with a pair of tuneable ECL lasers (IDPhotonics CoBrite DX2-S) separated by the corresponding LO frequency. The bias of the MUTC-PD is set at -2 V. The optical power at the input of the lensed fibre after the EDFA (Keopsys CEFA-CE-BO-HP) was measured at

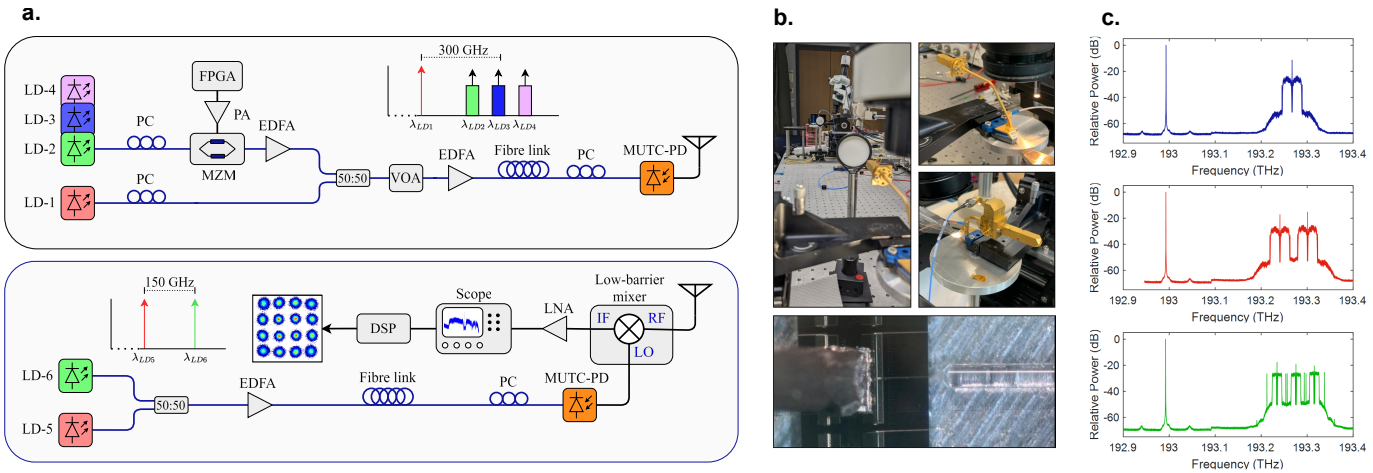

Fig. 2. Experimental arrangement: **a.** System schematic of the 300 GHz communications experiment. The THz multi-channel transmission (top) is achieved by optical heterodyning in a MUTC-PD with multiple free-running lasers modulated in intensity with an MZM. In the receiver (bottom), two free-running lasers separated by the desired frequency are heterodyned in a second MUTC-PD pumping the low-barrier mixer. The down-converted signal is amplified by an LNA and captured with the scope to apply an offline DSP routine. **b.** Photographies of the setup arrangement, from top to bottom and left to right: wireless link seen from the transmitter, photomixer-based transmitter, optically-pumped low-barrier mixer, microscope view of the transmitter MUTC-PD probing and fibre coupling. **c.** Example of optical spectrums at the transmitter side for the single-channel, dual-channel and triple-channel scenarios. LD: Laser diode, PC: Polarization controller, FPGA: Field programmable gate array, PA: Power amplifier, EDFA: Erbium-doped fibre amplifier, VOA: Variable optical attenuator, MUTC-PD: Modified uni-travelling-carrier photodiode, LNA: Low-noise amplifier, DSP: Digital signal processing.

23 dBm. In this case, we use a GSG WR6 probe connected to the input LO port of the low-barrier mixer (see figure 2.**b**.middle-right). The incoming RF signal is coupled to the mixer after propagating 1.5 m with a 5 cm PTFE lens and WR3.4 horn antenna.

The down-converted IF signal is amplified with a 40 dB gain low-noise-amplifier (LNA) (RF-Lambda RLNA00G30GA) and then digitized with an 80 Gsamples/s oscilloscope (Agilent DSO-X 933304Q) capturing sequences of 25 µs length. That results in a minimum measurable bit-error-rate (BER) of $4 \cdot 10^{-6}$ for a 10 Gbps signal. In figure 3 two examples of the received IF power spectrums are depicted corresponding to a 12.5 Gbaud signal (3.**a.**) and a 25 Gbaud signal (3.**b.**). The spectrums reveal three aspects: the signal-signal-beating interference (SSBI) [50], the out-of-band IF effects, and the cut-off of the scope (33 GHz). Note that the 25 Gbaud signal (100 Gbps) occupies frequencies beyond the IF bandwidth of the low-barrier mixer ($\sim$ 23 GHz) and also suffers from SSBI. This effect arises from the beating between the upper and lower optical sidebands (see figure 2.**c.**) due to the square-law type detection of the MUTC-PD transmitter [51].

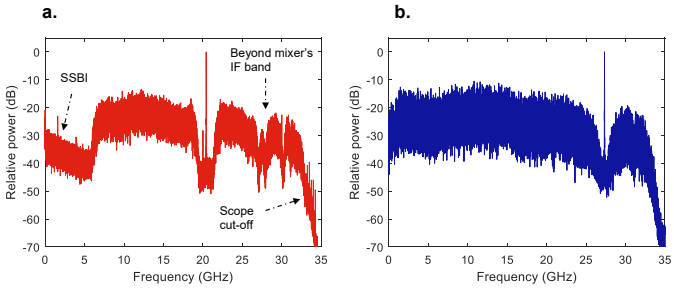

Fig. 3. Example of captured IF power spectrums showing the upconverted waveforms of 12.5 (**a.**) and 25 Gbaud (**b.**) signals. The obtained spectra provide insights into three important aspects: signal-signal-beating interference (SSBI), out-of-band IF effects, and the scope's cut-off.

C. Digital signal processing routine

The digitized IF signal goes through a coherent digital signal processing (DSP) routine (offline) to retrieve the data sequence. The steps are summarized in figure 4.**a.** and detailed here:

- First, the clock of the signal is recovered by performing a cross-correlation with the digital IQ upconverted waveform used in the transmitter DSP. Then the signal is down-converted to baseband. In this case frequency-offset corrections are not needed because the centre frequency is accurately known thanks to the presence of the carrier. This down-conversion is done considering the lower sideband (LSB) by default, but it can also be done by adding the upper side band (USB). The baseband signal is filtered with an inverse RC filter ($\alpha = 0.1$) and resampled at 2 samples per symbol.
- A set of three blind digital equalizers are used: radius-directed equalizer (RDE), carrier phase estimation (CPE), and the classic least-mean-square decision-directed equalizer (LMS-DDE). The RDE algorithm is used due to its overall better performance than other techniques like the constant modulus algorithm (CMA) in 16-QAM signals [52]. The DDE helps to further reduce the bit error rate. For instance, we measured a 150 % BER improvement when including the DDE for 100 Gbps transmission. Finally, the CPE algorithm is critical as it needs to compensate for the combined phase noise of the free-running lasers used in the transmitter and the receiver. For this purpose, we use the algorithm proposed in [53] which is based on a feed-forward architecture. The algorithm is robust against laser line widths of several MHzs.
- After the equalizers, the recovered symbols are mapped to bits and synchronized with the transmitted sequence. In the last step, the BER and EVM are calculated and

the SNR is estimated from the BER result.

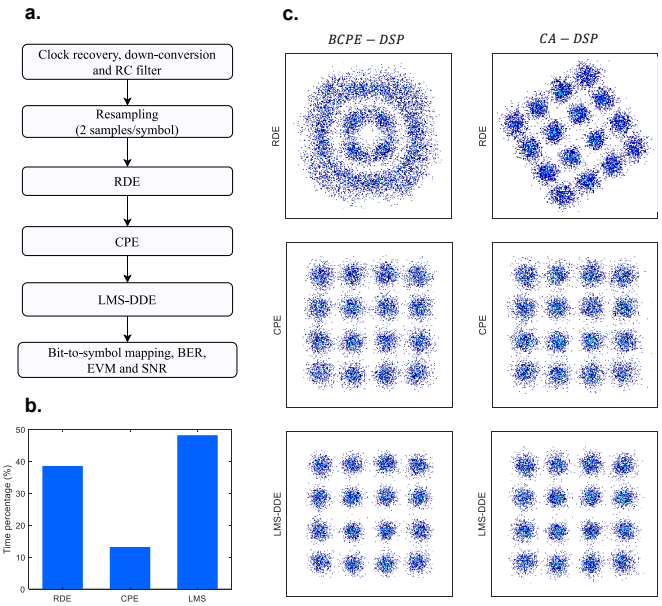

Fig. 4. Rx DSP insights: **a.** Sequential steps of the DSP. **b.** Mean time percentage spent on each equalizer. **c.** Example of a 10000 symbol input block processed with the carrier-assisted technique and with the blind phase estimation.

The relative time spent in each equalizer is shown in figure 4.**b.** This DSP routine can retrieve coherent data using non-locked optical sources at both the transmitter and receiver. However, as optical intensity modulation is used in the transmitter, the intrinsic carrier can be used to cancel phase noise. To do this, the carrier and one of the sidebands are filtered and mixed digitally, canceling common phase noise as a result. This would be similar to the pilot-tone-assisted technique proposed in [54] but using the intrinsic carrier in the system. We refer to this approach as the Carrier-assisted DSP (CA-DSP), and to Blind Carrier Phase Estimation DSP (BCPE-DSP) in the opposite case. In figure 4.**c.** an example of a 10000 symbol block after each DSP equalizer is shown using both techniques. In both cases, phase noise is effectively reduced. In the CA-DSP, the phase noise is not present after the RDE, requiring only a fixed rotation to be applied.

D. Measurements

Using the experimental configuration previously outlined, we performed a set of measurements as detailed here. The transmitted RF frequencies for each case are summarized in table II. The minimum frequency channel separation, denoted by Δf, is established as $\Delta f = 3\,(R_s{+}1.5)$ GHz to prevent image frequency interference. In the scenario with two channels, frequency separation of $\Delta f = 2\,(R_s + 1.5)$ GHz could suffice to avoid interference. We maintained the additional separation to utilize the optimal LO range of the low-barrier mixer in the receiver, approximately ranging from 130 to 150 GHz. Furthermore, in the two-channel scenario, the centre frequencies were adjusted for faster signals (symbol rate greater than 10 Gbaud) to accommodate their bandwidth.

For each multi-channel scenario, we transmitted 16-QAM waveforms of increasing data rates as follows: 10 to 100 Gbps in 10 Gbps steps for one channel, 10 to 90 Gbps in 10 Gbps steps for two channels, and 5, 10, 20, 30, and 35 Gbps for three channels. Each channel is received and sampled sequentially by tuning the photonic LO of the receiver. In addition, the photocurrent at both the MUTC-PD at the transmitter and receiver is optimized. At the transmitter, the goal is to achieve a balance between emitted power and non-linearities in the system. On the receiver side, optimum photocurrent means providing sufficient LO power to saturate conversion loss, leading to improved receiver sensitivity and overall performance. In addition to BER and EVM, which are measured by comparing retrieved and transmitted sequences, the SNR is estimated from the BER result as follows for 16-QAM format [55]

TABLE II
SUMMARY OF FREQUENCIES USED IN THE MULTI-CHANNEL LINK.

Number of channels	RF frequency (GHz)	LO frequency (GHz)*
1	270	145
2	250, 300 ($R_s \leq 10$ Gbaud) 240, 315 ($R_s > 10$ Gbaud)	135, 140 130, 147.5
3	240, 280, 320	130, 140, 150

*The LO frequency corresponds to a down-converted IF frequency of 10-20 GHz.

$$\mathrm{SNR(dB)} = 20\log_{10}\left(\sqrt{10\cdot \mathrm{erfc}^{-1}(8/3\cdot \mathrm{BER})}\right) \quad (1)$$

where erfc^{-1} is the inverse error function. With the SNR several penalties can be calculated in dB. Specifically, this refers to the penalty associated with the BCPE-DSP in comparison to the CA-DSP, and the penalty associated with the use of multiple channels for the same aggregate data rate. For the CA-DSP, it is important to keep track of the carrier-to-sideband power ratio (CSPR), which is calculated as follows

$$\mathrm{CSPR} = \frac{\mathrm{RMS}(C_a(t))^2}{\mathrm{RMS}(\mathrm{LSB}(t))^2} \quad (2)$$

where RMS is the root-mean-square value function, $C_a(t)$ is the filtered carrier, and LSB(t) is the filtered lower sideband. It is worth mentioning that in this study we use the BCPE-DSP by default and the CA-DSP is only used for comparison. The goal here is to demonstrate a system that would also work with optical IQ modulation using free-running lasers. To investigate non-linearity effects in the presence of multiple frequency channels, we also transmit a 5 Gbps signal and vary the MUTC-PD transmitter photocurrent from 2.5 to 12 mA in 0.5 mA increments when using one, two, and three channels.

E. Link budget estimations

In order to evaluate how the link could be escalated in distance, we also performed link budget calculations by including commercial THz amplifiers and increasing lens diameters up to 60 cm. We did this in three different scenarios: (1) the current system, (2) THz amplification in the receiver, and (3) THz amplification in the transmitter and receiver. Assuming the received power and noise to be the limiting factor, the distance

can be improved by: (1) increasing the emitted power, (2) reducing the noise figure of the receiver, and (3) increasing the transmitter/receiver's antenna/lens gain. Therefore, we calculate the free-space path loss (FSPL) and noise figure for the conditions of this experiment and compare it with the values obtained by incorporating these improvements using the standard Friis equations.

TABLE III
TERAHERTZ COMPONENTS AND PARAMETERS USED FOR LINK BUDGET CALCULATIONS.

Component	Manufacturer	Part name	Frequency (GHz)	Gain (dB)	Noise figure (dB)	Psat (dBm)
TX amplifier	Fraunhofer IAF	M260AMPH	280-330	18	-	5
RX amplifier	VDI	WR3.4AMP-LN	220-330	14	9	-
RX mixer	ACST	310A	270-320	-16	16	-
IF amplifier	RF-Lambda	RLNA00G30GA	0.01-30	38	3	24

TABLE IV
SCENARIOS CONSIDERED FOR THE LINK BUDGET CALCULATIONS.

Case	RX amplification	TX amplification	TX gain (dB)*1	RX noise figure (dB)*2
1	No	No	-	19
2	Yes	No	-	10.4
3	Yes	Yes	18	10.4

*1 Considering an MUTC-PD output power of -18 dBm the power after the transmitter amplifier is 0 dBm which is lower than P_{sat}. *2 The noise figure is calculated with the values of table III and the Friis equation of noise figure.

The gain of the lens is assumed to increase linearly with its area and an additional attenuation by atmospheric absorption of 5 dB/km is considered [56]. In table III the relevant receiver components and their parameters used in the calculations are shown. The three studied cases are described in table IV including the transmitter gain and receiver noise figure.

III. RESULTS

The main results of the experiments are summarized in figure 5. Some retrieved constellations are plotted in figure 5.**b.**, showing two examples for each multi-channel scenario. In figure 5.**a.** the BER results are shown, where the HD-FEC ($3.84 \cdot 10^{-3}$, 6.7 % overhead) [57] and SD-FEC ($1.94 \cdot 10^{-2}$, 15.3 % overhead) [58] thresholds are highlighted. For the single channel case, data rates up to 80 Gbps remain below the HD-FEC limit and we are able to transmit a 100 Gbps signal below SD-FEC. The main limiting factor here is the IF bandwidth of the low-barrier mixer (23 GHz). In the two-channel scenario, up to 180 Gbps under the SD-FEC limit are transmitted, resulting in a maximum net data rate of 156 Gbps. Notice how the performance is better for the lower frequency channel, up to 100 Gbps, due to the equal power of the two modulated lasers. This results in the higher THz channel having reduced power due to the MUTC-PD roll-off. However, beyond 100 Gbps, the power of the modulated lasers was tuned to compensate for this effect and achieve equal BER. When employing three channels, up to an aggregate 105 Gbps rate is achieved under the SD-FEC limit. In this case, the power of the modulated lasers was compensated for all data rates. Having unequal power between lasers introduces a certain level of EDFA gain competition. Since the aim of compensation is to balance the BER across channels, this effect is already accounted for. The photocurrent of the MUTC-PD transmitter was set to 10 mA for single and dual channel scenarios by keeping the same the input optical power. In the triple channel case, the photocurrent was reduced to 8 mA to mitigate non-linear effects. The photocurrent was limited due to the saturation of the low-barrier mixer, which occurs when the RF power is about 10 dB lower than the LO power. Since we were driving the mixer with approximately -7 dBm of LO power to achieve optimal conversion loss, the received RF power is estimated to be around -18 dBm, as FSPL is compensated with the THz lenses. The 1 dB power compression point for 5x30 μm^2 MUTC-PD devices has been measured to be at approximately 15 mA for 320 GHz [44]. Even though the MUTC-PD transmitter is expected be in linear regime at 10 mA, a certain level of non-linearity in the transmission can be attributed to it.

In figure 6.**a.** and 6.**b.** the average SNR and EVM are shown for each case. A degradation of performance for the same data rate can be observed when increasing the number of channels, particularly when looking at the SNR at low baud rates. This is expected as a result of non-linearities, and its effects can be visually noticed at the compression of higher energy symbols (figure 5.**b.**). A better evaluation of this impairment is extracted from the penalty calculation, shown in figure 6.**d.** based on SNR comparison. A maximum penalty of 1 and 2.5 dB are obtained for the two-channel and three-channel scenarios respectively. This degradation is less significant for increasing data rate, exhibiting a negative penalty for rates beyond 80 Gbps. This occurs because, for increasing data rate, the IF signal approaches or goes beyond the IF bandwidth of the low-barrier mixer, e.g. in the 100 Gbps case, the IF signal occupies frequencies higher than 25 GHz. A slight penalty is observed when using the CA-DSP (figure 6 **c.**), typically less than 1 dB. The penalty seems to be relatively insensitive to CSPR, with a modest improvement for decreasing CSPR. This can be attributed to less robustness against SSBI for increasing baud rates [59]. Further theoretical analysis would be required to determine the optimum value of CSPR for the CA-DSP technique which is not based on envelope detection such as the Kramers-Kronig technique. The CSPR is typically less than -10 dB which indicates that the carrier does not contribute significantly to signal saturation. The performance degradation when using three channels is also associated with extending the maximum operating frequency to 320 GHz, which negatively impacts the mixer's performance.

Regarding saturation effects, in figure 7 the BER and EVM are depicted for increasing photocurrent at the MUTC-PD transmitter for a 5 Gbps waveform. In the two and three-channel scenarios, the BER and EVM are calculated by averaging the values measured for each channel. These results highlight how non-linearities become more relevant for an increasing number of channels. The BER and EVM saturate at approximately 6.5, 7.5, and 9.5 mA for single, dual, and triple channel scenarios respectively. An offset in performance for an increasing number of channels is expected as the aggregate data rate is higher. The difference in saturation point can

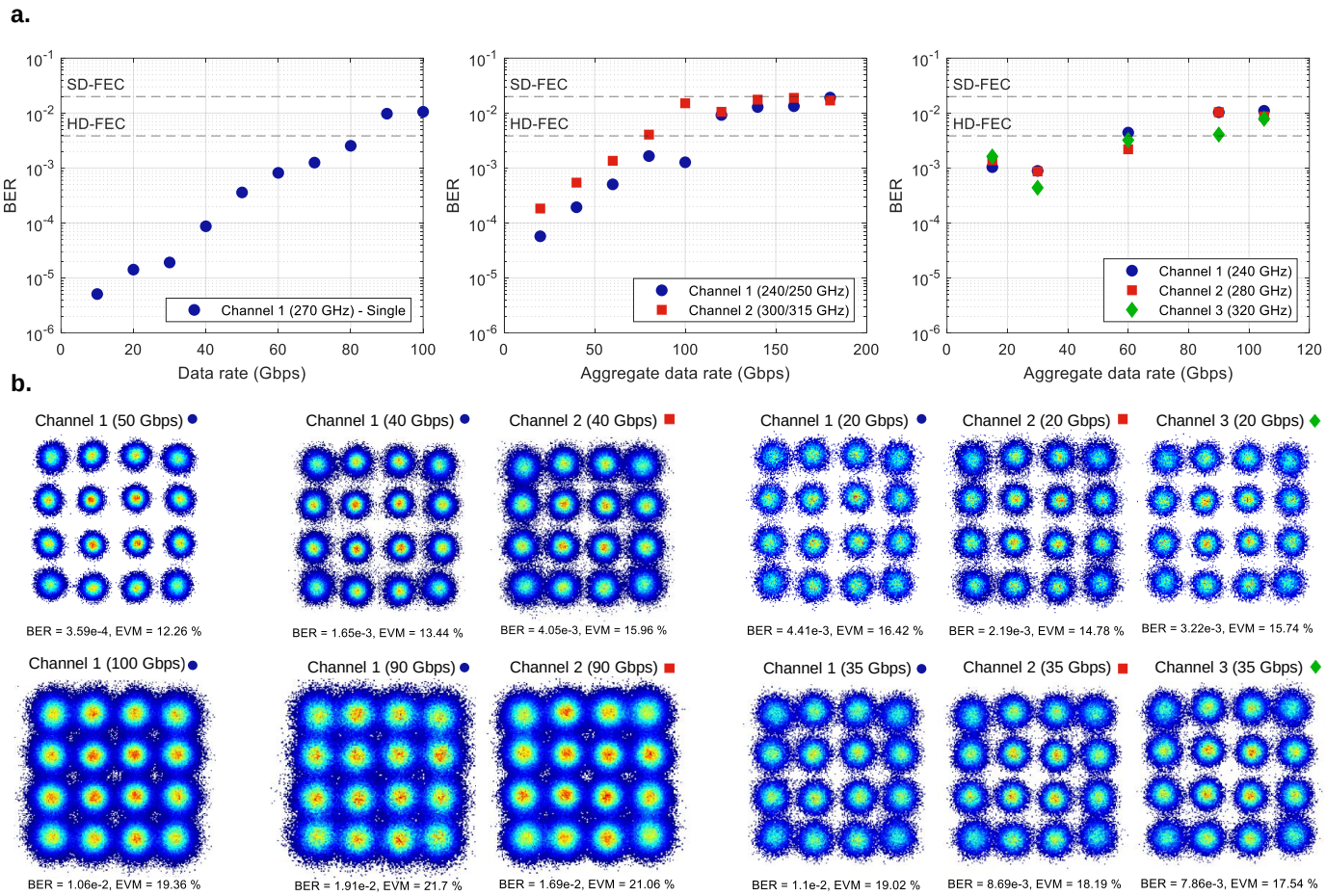

Fig. 5. Main results of the 300 GHz communications experiment: **a.** BER vs data rates for the different multi-channel scenarios. The lines depicting HD-FEC and SD-FEC correspond to $3.84 \cdot 10^{-3}$ and $1.94 \cdot 10^{-2}$ thresholds with 6.7 % and 15.3 % overhead respectively. The data rate corresponds to the aggregate throughput between channels. **b.** Examples of recovered constellations at two data rates for each scenario (single, dual, and triple channel) from left to right. In the two-channel scenario, the centre frequencies of channels 1 and 2 were changed from 250 and 300 GHz, to 240 and 315 GHz when transmitting signals with a symbol rate greater than 10 Gbaud (40 Gbps), as highlighted in table II. The photocurrent of the MUTC-PD transmitter is set to 10 mA in both single and dual-channel scenarios, maintaining the same optical input power. This is reduced to 8 mA in the triple-channel case.

be attributed to a reduced tolerance to non-linearities when having more channels. As the number of channels increases, intermodulation between them becomes more pronounced, degrading the performance. Fewer channel transmission can tolerate a certain level of saturation as the trade-off between SNR and intermodulation distortion is better.

Finally, link budget estimations for a single channel are shown in figure 8. The calculated curves represent the achievable distance in each case for different antenna/lens diameters. This is achieved by maintaining the same SNRs in the experiment, compensating for the increase in FSPL and attenuation through improvements in transmitter and receiver gain, as well as the noise figure. Consequently, the BER and EVM values for each data rate are preserved. Distances of up to 1.7 km could be potentially achieved with THz amplifiers in both transmitter and receiver and an increased antenna/lens diameter of 60 cm.

IV. Discussion

The performance achieved in these experiments represents a breakthrough for fully-optoelectronic links, thanks to the novel low-barrier Schottky mixer driven with the MUTC-PD. The conversion loss of the mixer, of the order of 15-20 dB [41], is far superior to the reported values for photoconductor-based receivers, the minimum conversion at 300 GHz being of the order of 30 dB [32], [34]. This figure, however, is typically higher, exceeding 60 dB in the highest data rate reported photoconductor-based receiver wireless THz link [24].

The low-barrier property of the InGaAs Schottky mixer is critical to be driven optically with a UTC-PD. Although it is possible to do the same with a classic GaAs mixer, the limited available power imposes a significant challenge. An illustrative case is found in [39], where the authors operated a subharmonic GaAs mixer at 262 GHz without achieving optimum LO power, compromising the performance of the link. The authors in [40] also use a GaAs mixer pumped with a W-band UTC-PD, including a power amplifier and a doubler, thereby increasing power consumption at the THz frontend and phase noise. The challenges associated with insufficient photomixer power become more severe at higher frequencies. Thus, employing a low-barrier mixer enables fully-optoelectronic links at these higher frequencies. In addition, reducing the required LO power has a direct impact in DC power consumption related to LO generation, which

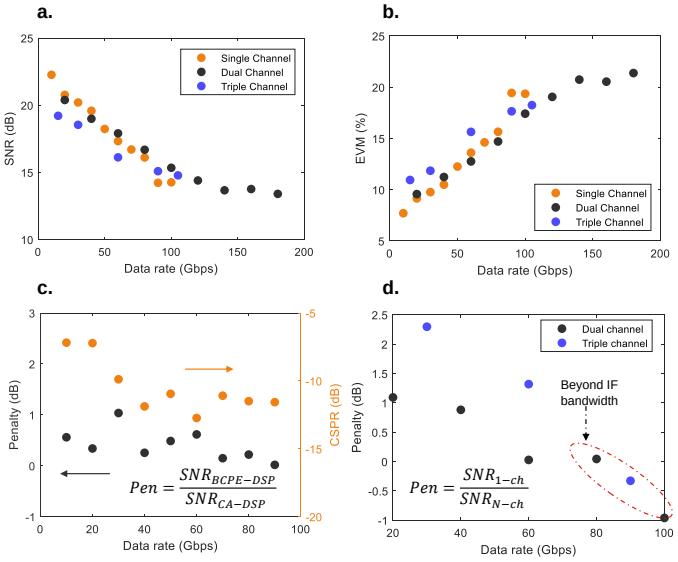

Fig. 6. Additional results: **a.** SNR comparison estimated from the BER measurements. The data rate corresponds to the aggregate throughput between channels. **b.** EVM comparison. **c.** Penalties associated with the receiver DSP with blind carrier phase estimation and carrier-assisted techniques in the single-channel case. **d.** Penalties associated with the transmission of multiple channels.

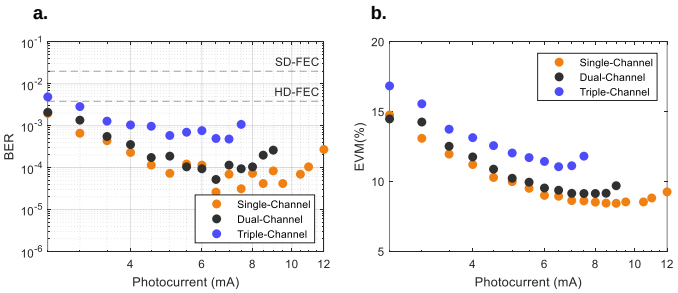

Fig. 7. Transmitter MUTC-PD photocurrent sweep measurements for a 1.25 Gbaud signal (i.e. 5, 10, and 15 Gbps aggregate data rates for single dual and triple-channel), showing **a.** BER, and **b.** EVM. The x-axis refers to the total PD photocurrent.

is directly proportional to the LO power. Therefore, a low-barrier mixer contributes to improve the power-efficiency of the system. In terms of conversion loss, while the low-barrier mixer is inferior compared to GaAs mixers, this is largely attributed to a less mature fabrication and design process for this particular mixer prototype. In principle, InGaAs could achieve similar performance than GaAs in a Schottky mixer [45], [46]. Moreover, the use of InGaAs enables the monolithic integration with UTC-PDs.

When compared to receivers based on photoconductors, the main limitation of our proposed optoelectronic solution is the frequency tuneability. In this case, it is constrained to $\sim$ 240-320 GHz although the mixer is designed for the narrow band 270-320 GHz. SBD-based mixers use filters and impedance-matching circuits which inevitably limits the operation bandwidth. However, in communications extreme frequency tuneability is arguably not required as future deployed terahertz links would likely stay within a limited frequency defined by the particular standard, for instance, 252-325 GHz in IEEE 802.15.3d [15]. In this sense, this demonstration almost covers

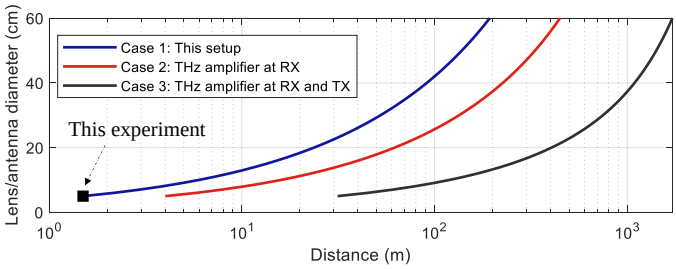

Fig. 8. Achievable distance according to link budget estimations by increasing lens diameter and incorporating THz amplifiers. The technical specification of the amplifiers can be found in table III.

the full bandwidth of the terahertz standard, which is limited not by the technology but by the design of the low-barrier mixer. In addition, for long-distance links, e.g. fronthaul or backhaul, amplification will be most likely necessary, which will intrinsically restrict the frequency range. We argue that the primary advantages of photonic local oscillator systems in terahertz communications are: (1) the agility of signal generation addressing multiple channel signals across a wide bandwidth, and (2) the distribution of both the transmitter and receiver LOs via optical fibre. Ultimately this will reduce the complexity of the THz wireless frontend and its energy consumption.

Direct THz-to-optical conversion with ultra-broadband plasmonic modulators is a compelling alternative that has demonstrated state-of-the-art transmission rates at 230 GHz [35]. However, a down-conversion scheme gives more flexibility considering that DRoF might still be the dominant solution in 6G. Moreoever, the throughput achieved in this work is comparable despite (1) using optical intensity modulation and upconverted QAM waveforms, and (2) avoiding terahertz amplification in the transmitter. Optical IQ modulation would provide higher spectral efficiency and potentially double the data rate as the terahertz power would be spread over half the frequency range. Increasing the emitted MUTC-PD power by using THz amplifiers would increase the achievable distance. Depending on the use case, intensity modulation could be preferred over IQ modulation, particularly when lower complexity is prioritized over throughput. We have also shown how the intrinsic carrier can be used to mitigate the impact of phase noise, reducing the DSP load. These points highlight the virtues of our system.

Regarding further improvements, the bandwidth bottleneck in the link is found in the SMA IF connector of the low-barrier mixer, limited to around 23 GHz. The use of a higher frequency connector, e.g. K or V connectors, would allow the data rate for a single channel to be higher with the current QAM order. Data rates could be further improved by using polarization multiplexing, which can be easily implemented by optical means with commercial dual-polarization IQ transmitters. These enhancements, together with optical IQ modulation, will improve the BER margin to the HD-FEC and SD-FEC limits, allowing transmission of more than 100 Gbps below the HD-FEC threshold. The distance, which in this case was limited to 1.5 m due to space constraints, could be significantly improved by adding terahertz amplifi-

cation and using bigger lenses/antennas as shown in the link budget estimations. These calculations assume the noise of the receiver to be dominant, neglect the non-linear effects of terahertz amplification and presume an ideal antenna/lens area and gain dependency. Therefore, they provide a conceptual overview of the potential capabilities of a link incorporating these enhancements and should be interpreted as such.

Finally, in this demonstration each channel is received and sampled sequentially. Although this is a standard approach in multi-channel terahertz communications [24], [60]–[62], simultaneous reception must be implemented in a real-world scenario. In this sense, if all channels are to be received in the same unit (point-to-point), terahertz demultiplexing could be used, which has already showed remarkable performance [63], [64]. Alternatively, if each channel is received by different units (point-to-multipoint), leaky-wave antennas could provide frequency-dependent link directions feeding multiple users [65], [66]. By using multi-carrier transmission, the total rate of the wireless link can be increased, as demonstrated here. The optimal number of channels depends on various factors, including the bandwidth of different components, nonlinearities, and the specific application. For instance, in a point-to-multipoint link, the number of users to serve determines the number of channels required. Another significant advantage of multi-carrier transmission is that it substantially reduces the required bandwidth for some critical components, such as digital-to-analog and analog-to-digital converters (DACs and ADCs) and low noise amplfiers (LNAs).

V. Conclusion

In the present study, an optoelectronic multi-channel 300 GHz link has been demonstrated. A maximum net data rate of 156 Gbps over 1.5 m has been achieved without terahertz amplification, with sequential channel reception. To the best of our knowledge, this is a record data rate not only for fully-optoelectronic THz communications based on a down-conversion scheme, but also for optical intensity modulation based THz communications. The combined use of a low-barrier Schottky mixer and a photonic LO generated in an MUTC-PD enables highly improved optoelectronic reception compared to photoconductor-based receivers. The low LO power requirement of the mixer also enables fully-optoelectronic links at higher frequencies and reduces the DC power consumption associated to LO generation. While the MUTC-PD and the Schottky mixer are separate components, they have the potential to be monolithically integrated as the mixer is based on InGaAs Schottky contacts, and therefore compatible with 1.55 um UTC-PDs epitaxial structures. Further improvements in the system such as optical IQ modulation or polarization multiplexing would enable data rates as high as the state-of-the-art levels. Basic link budget estimations suggest that over one kilometer links could be feasible with terahertz amplification, which is now commercially available at 300 GHz. In this work, we have shown how a fully-optoelectronic link can compete with systems based on electronic LO receivers. Our solution enables multi-channel 300 GHz communications with reduced THz front-end power-consumption and complexity, and seamless convergence with fibre networks. These reasons make the proposed system a relevant candidate for wireless fronthaul and backhaul in future 6G and beyond networks.

Acknowledgment

The authors would like to thank Dr. Luis Gonzalez-Guerrero for his contribution to the MATLAB code of the DSP equalizers.

References

[1] H.-J. Song and N. Lee, "Terahertz communications: Challenges in the next decade," *IEEE Transactions on Terahertz Science and Technology*, vol. 12, no. 2, pp. 105–117, Mar. 2022.

[2] Z. Chen, X. Ma, B. Zhang, Y. Zhang, Z. Niu, N. Kuang, W. Chen, L. Li, and S. Li, "A survey on terahertz communications," *China Communications*, vol. 16, no. 2, pp. 1–35, Feb. 2019.

[3] T. Kürner, D. M. Mittleman, and T. Nagatsuma, *THz Communications: Paving the Way Towards Wireless Tbps*. Springer Nature, Dec. 2021.

[4] H. Cho, S. Mukherjee, D. Kim, T. Noh, and J. Lee, "Facing to wireless network densification in 6g: Challenges and opportunities," *ICT Express*, vol. 9, no. 3, pp. 517–524, Jun. 2023.

[5] H. Saarnisaari, A. Chaoub, M. Heikkilä, A. Singhal, and V. Bhatia, "Wireless terrestrial backhaul for 6G remote access: Challenges and low power solutions," *Frontiers in Communications and Networks*, vol. 2, 2021.

[6] G. Kalfas, C. Vagionas, A. Antonopoulos, E. Kartsakli, A. Mesodiakaki, S. Papaioannou, P. Maniotis, J. S. Vardakas, C. Verikoukis, and N. Pleros, "Next generation Fiber-Wireless fronthaul for 5G mmwave networks," *IEEE Commun. Mag.*, vol. 57, no. 3, pp. 138–144, Mar. 2019.

[7] T. Kawanishi, "THz and photonic seamless communications," *J. Lightwave Technol.*, vol. 37, no. 7, pp. 1671–1679, 2019.

[8] A. Kanno, P. Tien Dat, N. Sekine, I. Hosako, T. Kawanishi, Y. Yoshida, and K. Kitayama, "High-speed coherent transmission using advanced photonics in terahertz bands," *IEICE Trans. Electron.*, vol. E98.C, no. 12, pp. 1071–1080, 2015.

[9] G.-K. Chang and L. Cheng, "The benefits of convergence," *Philos. Trans. A Math. Phys. Eng. Sci.*, vol. 374, no. 2062, Mar. 2016.

[10] J. M. Eckhardt and T. Doeker, "Data centers," in *THz Communications: Paving the Way Towards Wireless Tbps*, T. Kürner, D. M. Mittleman, and T. Nagatsuma, Eds. Cham: Springer International Publishing, 2022, pp. 131–138.

[11] S. Mollahasani and E. Onur, "Evaluation of terahertz channel in data centers," in *NOMS 2016 - 2016 IEEE/IFIP Network Operations and Management Symposium*, Apr. 2016, pp. 727–730.

[12] A. S. Hamza, J. S. Deogun, and D. R. Alexander, "Wireless communication in data centers: A survey," *IEEE Communications Surveys & Tutorials*, vol. 18, no. 3, pp. 1572–1595, 2016.

[13] E. Baccour, S. Foufou, R. Hamila, and M. Hamdi, "A survey of wireless data center networks," in *2015 49th Annual Conference on Information Sciences and Systems (CISS)*, Mar. 2015, pp. 1–6.

[14] A. Celik, B. Shihada, and M.-S. Alouini, "Wireless data center networks: Advances, challenges, and opportunities," *arXiv preprint arXiv:1811.11717*, Nov. 2018.

[15] V. Petrov, T. Kurner, and I. Hosako, "IEEE 802.15.3d: First standardization efforts for Sub-Terahertz band communications toward 6G," *IEEE Commun. Mag.*, vol. 58, no. 11, pp. 28–33, Nov. 2020.

[16] I. Kallfass, I. Dan, S. Rey, P. Harati, J. Antes, A. Tessmann, S. Wagner, M. Kuri, R. Weber, H. Massler, A. Leuther, T. Merkle, and T. Kürner, "Towards MMIC-Based 300GHz indoor wireless communication systems," *IEICE Transactions on Electronics*, vol. E98.C, no. 12, pp. 1081–1090, 2015.

[17] S. Lee, S. Hara, T. Yoshida, S. Amakawa, R. Dong, A. Kasamatsu, J. Sato, and M. Fujishima, "An 80-gb/s 300-GHz-Band Single-Chip CMOS transceiver," *IEEE J. Solid-State Circuits*, vol. 54, no. 12, pp. 3577–3588, Dec. 2019.

[18] H. Hamada, T. Fujimura, I. Abdo, K. Okada, H.-J. Song, H. Sugiyama, H. Matsuzaki, and H. Nosaka, "300-GHz. 100-gb/s InP-HEMT wireless transceiver using a 300-GHz fundamental mixer," in *2018 IEEE/MTT-S International Microwave Symposium - IMS*, Jun. 2018, pp. 1480–1483.

[19] P. Sen, J. V. Siles, N. Thawdar, and J. M. Jornet, "Multi-kilometre and multi-gigabit-per-second sub-terahertz communications for wireless backhaul applications," *Nature Electronics*, vol. 6, no. 2, pp. 164–175, Dec. 2022.

[20] S. Koenig, D. Lopez-Diaz, J. Antes, F. Boes, R. Henneberger, A. Leuther, A. Tessmann, R. Schmogrow, D. Hillerkuss, R. Palmer, T. Zwick, C. Koos, W. Freude, O. Ambacher, J. Leuthold, and I. Kallfass, "Wireless sub-THz communication system with high data rate," *Nat. Photonics*, vol. 7, no. 12, pp. 977–981, Oct. 2013.

[21] S. Wang, Z. Lu, W. Li, S. Jia, L. Zhang, M. Qiao, X. Pang, N. Idrees, M. Saqlain, X. Gao, X. Cao, C. Lin, Q. Wu, X. Zhang, and X. Yu, "26.8-m THz wireless transmission of probabilistic shaping 16-QAM-OFDM signals," *APL Photonics*, vol. 5, no. 5, p. 056105, May 2020.

[22] Jia, Zhang, Wang, Li, Qiao, Lu, and others, "2× 300 gbit/s line rate PS-64QAM-OFDM THz photonic-wireless transmission," *J. Lightwave Technol.*, 2020.

[23] W. Li, J. Yu, B. Zhu, J. Zhang, M. Zhu, F. Zhao, T. Xie, K. Wang, Y. Wei, X. Yang, B. Hua, M. Lei, Y. Cai, W. Zhou, and J. Yu, "Photonics-assisted 320 GHz THz-band 50 gbit/s signal outdoor wireless communication over 850 meters," in *2023 Optical Fiber Communications Conference and Exhibition (OFC)*, Mar. 2023, pp. 1–3.

[24] T. Harter, S. Ummethala, M. Blaicher, S. Muehlbrandt, S. Wolf, M. Weber, M. M. H. Adib, J. N. Kemal, M. Merboldt, F. Boes, S. Nellen, A. Tessmann, M. Walther, B. Globisch, T. Zwick, W. Freude, S. Randel, and C. Koos, "Wireless THz link with optoelectronic transmitter and receiver," *Optica*, vol. 6, no. 8, p. 1063, Aug. 2019.

[25] A. Morales, G. Nazarikov, S. Rommel, C. Okonkwo, and I. T. Monroy, "Highly tunable heterodyne Sub-THz wireless link entirely based on optoelectronics," *IEEE Transactions on Terahertz Science and Technology*, vol. 11, no. 3, pp. 261–268, May 2021.

[26] E. Andrianopoulos, N. K. Lyras, E. Pikasis, G. Schwanke, M. Deumer, S. Nellen, T. Qian, G. D. Ntouni, E. C. Loghis, E. D. Tsirbas, P.-K. Chartsias, D. De Felipe, P. Groumas, M. Massaouti, C. Tsokos, C. Kouloumentas, D. Kritharidis, R. B. Kohlhaas, N. Keil, M. Schell, and H. Avramopoulos, "Real-Time Sub-THz link enabled purely by optoelectronics: 90–310 GHz seamless operation," *IEEE Photonics Technol. Lett.*, vol. 35, no. 5, pp. 237–240, Mar. 2023.

[27] T. Nagatsuma, G. Ducournau, and C. C. Renaud, "Advances in terahertz communications accelerated by photonics," *Nat. Photonics*, vol. 10, no. 6, pp. 371–379, 2016.

[28] H. Zhang, L. Zhang, S. Wang, Z. Lu, Z. Yang, S. Liu, M. Qiao, Y. He, X. Pang, X. Zhang, and X. Yu, "Tbit/s Multi-Dimensional multiplexing THz-Over-Fiber for 6G wireless communication," *J. Lightwave Technol.*, vol. 39, no. 18, pp. 5783–5790, Sep. 2021.

[29] D. Stanze, A. Deninger, A. Roggenbuck, S. Schindler, M. Schlak, and B. Sartorius, "Compact cw terahertz spectrometer pumped at 1.5 μm wavelength," *J. Infrared Millim. Terahertz Waves*, vol. 32, no. 2, pp. 225–232, Feb. 2011.

[30] L. Liebermeister, S. Nellen, R. B. Kohlhaas, S. Lauck, M. Deumer, S. Breuer, M. Schell, and B. Globisch, "Optoelectronic frequency-modulated continuous-wave terahertz spectroscopy with 4 THz bandwidth," *Nat. Commun.*, vol. 12, no. 1, 2021.

[31] M. Deumer, S. Breuer, R. Kohlhaas, S. Nellen, L. Liebermeister, S. Lauck, M. Schell, and B. Globisch, "Continuous wave terahertz receivers with 4.5 THz bandwidth and 112 db dynamic range," *Opt. Express*, vol. 29, no. 25, pp. 41 819–41 826, Dec. 2021.

[32] E. Peytavit, F. Pavanello, G. Ducournau, and J.-F. Lampin, "Highly efficient terahertz detection by optical mixing in a GaAs photoconductor," *Appl. Phys. Lett.*, vol. 103, no. 20, p. 201107, 2013.

[33] C. C. Renaud, M. Natrella, C. Graham, J. Seddon, F. Van Dijk, and A. J. Seeds, "Antenna integrated THz Uni-Traveling carrier photodiodes," *IEEE J. Sel. Top. Quantum Electron.*, vol. 24, no. 2, pp. 1–11, Mar. 2018.

[34] C. Tannoury, V. Merupo, G. Di Gioia, V. Avramovic, D. Troadec, J.-F. Lampin, G. Ducournau, S. Breuer, B. Globisch, S. Barbieri, R. B. Kohlhaas, and E. Peytavit, "Photonic THz mixers based on iron-doped InGaAs embedded in a plasmonic microcavity," *APL Photonics*, vol. 8, no. 11, Nov. 2023.

[35] Y. Horst, T. Blatter, L. Kulmer, B. I. Bitachon, B. Baeuerle, M. Destraz, W. Heni, S. Koepfli, P. Habegger, M. Eppenberger, E. De Leo, C. Hoessbacher, D. L. Elder, S. R. Hammond, L. E. Johnson, L. R. Dalton, Y. Fedoryshyn, Y. Salamin, M. Burla, and J. Leuthold, "Transparent Optical-THz-Optical link at 240/192 gbit/s over 5/115 m enabled by plasmonics," *J. Lightwave Technol.*, vol. 40, no. 6, pp. 1690–1697, 2022.

[36] M. Deumer, L. Liebermeister, O. Stiewe, S. Nellen, R. B. Kohlhaas, R. Elschner, C. Schubert, R. Freund, and M. Schell, "Purely photonic wireless link at 120 GHz with a photoconductive antenna as heterodyne receiver," in *2023 48th International Conference on Infrared, Millimeter, and Terahertz Waves (IRMMW-THz)*. IEEE, Sep. 2023, pp. 1–2.

[37] M. Deumer, O. Stiewe, S. Nellen, S. Lauck, S. Breuer, R. B. Kohlhaas, C. Schubert, R. Elschner, R. Freund, and M. Schell, "Optoelectronic heterodyne THz receiver for 100–300 GHz communication links," *IEEE Access*, vol. 12, pp. 27 158–27 166, 2024.

[38] J. Dittmer, J. Tebart, C. Füllner, C. Koos, A. Stöhr, and S. Randel, "200 gbit/s wireless THz transmission over 52m using optoelectronic signal generation," in *2023 53rd European Microwave Conference (EuMC)*. IEEE, Sep. 2023, pp. 134–137.

[39] S. Cho, S.-R. Moon, M. Sung, S.-H. Cho, T. Kawanishi, and H.-J. Song, "A 262-GHz wireless IFoF uplink with remote Down-Conversion using optically generated Sub-THz LO," *IEEE Trans. Microw. Theory Tech.*, vol. 71, no. 5, pp. 2276–2285, May 2023.

[40] P. T. Dat, I. Morohashi, N. Sekine, A. Kanno, N. Yamamoto, and K. Akahane, "Fiber-terahertz-fiber bridge system in the 355-GHz band using a simple optical frequency comb and a photonics-enabled receiver," *Opt. Lett.*, vol. 48, no. 8, pp. 2190–2193, Apr. 2023.

[41] I. Belio-Apaolaza, J. Seddon, D. Moro-Melgar, H. P. Indiran, C. Graham, K. Balakier, O. Cojocari, and C. C. Renaud, "Photonically-driven schottky diode based 0.3 THz heterodyne receiver," *Opt. Express*, vol. 30, no. 24, pp. 43 223–43 236, Nov. 2022.

[42] S. Makhlouf, J. Martinez-Gil, M. Grzeslo, D. Moro-Melgar, O. Cojocari, and A. Stöhr, "High-power UTC-photodiodes for an optically pumped subharmonic terahertz receiver," *Opt. Express*, vol. 30, no. 24, pp. 43 798–43 814, Nov. 2022.

[43] M. Grzeslo, S. Dülme, S. Clochiatti, T. Neerfeld, T. Haddad, P. Lu, J. Tebart, S. Makhlouf, C. Biurrun-Quel, J. L. Fernández Estévez, J. Lackmann, N. Weimann, and A. Stöhr, "High saturation photocurrent THz waveguide-type MUTC-photodiodes reaching mw output power within the WR3.4 band," *Opt. Express*, vol. 31, no. 4, pp. 6484–6498, Feb. 2023.

[44] E. Abacıoğlu, M. Grzeslo, T. Neerfeld, J. L. F. Estévez, and A. Stöhr, "High output power broadband 1.55 μm Waveguide-Integrated terahertz MUTC-Photodiodes," in *2023 23rd International Conference on Transparent Optical Networks (ICTON)*. IEEE, Jul. 2023, pp. 1–4.

[45] Pardo, Wang, Sanghera, Alderman, and others, "InGaAs schottky technology for THz mixers," *Proc. 28th Int. Symp*, 2017.

[46] I. Oprea, A. Walber, O. Cojocari, H. Gibson, R. Zimmermann, and H. L. Hartnagel, "183 GHz mixer on InGaAs schottky diodes," *21ST INTERNATIONAL SYMPOSIUM ON SPACE TERAHERTZ TECHNOLOGY*, 2010.

[47] S. Khanal, T. Kiuru, M. Hoefle, J. Montero, O. Cojocari, J. Mallat, P. Pironen, and A. V. Räisänen, "Characterisation of low-barrier schottky diodes for millimeter wave mixer applications," in *2016 Global Symposium on Millimeter Waves (GSMM) & ESA Workshop on Millimetre-Wave Technology and Applications*. IEEE, Jun. 2016, pp. 1–4.

[48] *RPG SHM – Full band Subharmonic Mixer*, Radiometer Physics, Aug. 2021.

[49] J. Martinez Gil, D. Moro-Melgar, A. Negrus, I. Oprea, and O. Cojocari, "Efficiency assessment of traditional GaAs and Low-Power InGaAs schottky diodes in Full-Band mixers at 0.3 THz," *Electronics*, vol. 12, no. 21, p. 4518, Nov. 2023.

[50] Z. Li, M. S. Erkılınç, S. Pachnicke, H. Griesser, R. Bouziane, B. C. Thomsen, P. Bayvel, and R. I. Killey, "Signal-signal beat interference cancellation in spectrally-efficient WDM direct-detection nyquist-pulse-shaped 16-QAM subcarrier modulation," *Opt. Express*, vol. 23, no. 18, pp. 23 694–23 709, Sep. 2015.

[51] L. Gonzalez-Guerrero and G. Carpintero, "Coherent photonic terahertz transmitters compatible with direct comb modulation," *Sci. Rep.*, vol. 12, no. 1, pp. 1–10, Jun. 2022.

[52] I. Fatadin, D. Ives, and S. J. Savory, "Blind equalization and carrier phase recovery in a 16-QAM optical coherent system," *J. Lightwave Technol.*, vol. 27, no. 15, pp. 3042–3049, Aug. 2009.

[53] T. Pfau, S. Hoffmann, and R. Noe, "Hardware-Efficient coherent digital receiver concept with feedforward carrier recovery for M -QAM constellations," *J. Lightwave Technol.*, vol. 27, no. 8, pp. 989–999, Apr. 2009.

[54] L. Gonzalez-Guerrero, H. Shams, I. Fatadin, J. E. Wu, M. J. Fice, M. Naftaly, A. J. Seeds, and C. C. Renaud, "Pilot-Tone assisted 16-QAM photonic wireless bridge operating at 250 GHz," *J. Lightwave Technol.*, vol. 39, no. 9, pp. 2725–2736, May 2021.

[55] X. Liu, "High-capacity long-haul optical fibre transmission," in *Optical Communications in the 5G Era*. Academic Press, Oct. 2021, pp. 185–232.

[56] P. Series, "Attenuation by atmospheric gases and related effects," *Recommendation ITU-R*, vol. 25, pp. 676–612, 2019.

[57] E. Agrell and M. Secondini, "Information-Theoretic tools for optical communications engineers," in *2018 IEEE Photonics Conference (IPC)*, Sep. 2018, pp. 1–5.

[58] C. Schow, M. Filer, and C. Doerr, "Coherent interconnects for data centers," in *Integrated Photonics for Data Communication Applications*, M. Glick, L. Liao, and K. Schmidtke, Eds. Elsevier, Jan. 2023, pp. 201–232.

[59] D. Lu, X. Zhou, J. Huo, J. Gao, Y. Yang, K. He, J. Yuan, K. Long, C. Yu, A. P. T. Lau, and C. Lu, "Theoretical CSPR analysis and performance comparison for four Single-Sideband modulation schemes with Kramers-Kronig receiver," *IEEE Access*, vol. 7, pp. 166 257–166 267, 2019.

[60] H. Shams, T. Shao, M. J. Fice, P. M. Anandarajah, C. C. Renaud, F. Van Dijk, L. P. Barry, and A. J. Seeds, "100 gb/s multicarrier THz wireless transmission system with high frequency stability based on a Gain-Switched laser comb source," *IEEE Photonics J.*, vol. 7, no. 3, pp. 1–11, Jun. 2015.

[61] X. Yu, S. Jia, H. Hu, M. Galili, T. Morioka, P. U. Jepsen, and L. K. Oxenløwe, "160 gbit/s photonics wireless transmission in the 300-500 GHz band," *APL Photonics*, vol. 1, p. 081301, Nov. 2016.

[62] X. Pang, S. Jia, O. Ozolins, X. Yu, H. Hu, L. Marcon, P. Guan, F. Da Ros, S. Popov, G. Jacobsen, M. Galili, T. Morioka, D. Zibar, and L. K. Oxenkwe, "260 gbit/s photonic-wireless link in the THz band," in *2016 IEEE Photonics Conference (IPC)*. IEEE, Oct. 2016, pp. 1–2.

[63] A. Kumar, M. Gupta, P. Pitchappa, N. Wang, P. Szriftgiser, G. Ducournau, and R. Singh, "Phototunable chip-scale topological photonics: 160 gbps waveguide and demultiplexer for THz 6G communication," *Nat. Commun.*, vol. 13, no. 1, p. 5404, Sep. 2022.

[64] W. Deng, L. Chen, H. Zhang, S. Wang, Z. Lu, S. Liu, Z. Yang, Z. Wang, S. Yuan, Y. Wang, R. Wang, Y. Yu, X. Wu, X. Yu, and X. Zhang, "On-chip polarization- and frequency-division demultiplexing for multidimensional terahertz communication," *Laser Photon. Rev.*, vol. 16, no. 10, p. 2200136, Oct. 2022.

[65] P. Lu, T. Haddad, J. Tebart, M. Steeg, B. Sievert, J. Lackmann, A. Rennings, and A. Stöhr, "Mobile THz communications using photonic assisted beam steering leaky-wave antennas," *Opt. Express*, vol. 29, no. 14, pp. 21 629–21 638, Jul. 2021.

[66] H. Guerboukha, R. Shrestha, J. Neronha, Z. Fang, and D. M. Mittleman, "Conformal leaky-wave antennas for wireless terahertz communications," *Communications Engineering*, vol. 2, no. 1, pp. 1–9, Apr. 2023.